Correlation of structural, magnetic and transport properties with the tolerance factor in a low-doped $La_{0.875}Sr_{0.125-x}Ca_xMnO_3$, ($0 \leq x \leq 0.125$) system: cross-over from Mott to Shklovskii–Efros variable range hopping conduction

2007 J. Phys.: Condens. Matter 19 266218

(http://iopscience.iop.org/0953-8984/19/26/266218)

IOP PUBLISHING JOURNAL OF PHYSICS: CONDENSED MATTER

J. Phys.: Condens. Matter **19** (2007) 266218 (13pp) doi:10.1088/0953-8984/19/26/266218

Correlation of structural, magnetic and transport properties with the tolerance factor in a low-doped $La_{0.875}Sr_{0.125-x}Ca_xMnO_3$, ($0 \leqslant x \leqslant 0.125$) system: cross-over from Mott to Shklovskii–Efros variable range hopping conduction

Esa Bose[1], S Karmakar[1], B K Chaudhuri[1,3], S Pal[2,4], C Martin[2], S Hébert[2] and A Maignan[2]

[1] Department of Solid State Physics, Indian Association for the Cultivation of Science, Kolkata-700032, India
[2] Laboratoire CRISMAT, UMR 6508 CNRS, ENSICAEN, 6 Bd du Maréchal Juin,14050 CAEN Cedex, France

E-mail: sspbkc@iacs.res.in (B K Chaudhuri)

Received 9 February 2007, in final form 4 May 2007
Published 15 June 2007
Online at stacks.iop.org/JPhysCM/19/266218

Abstract

Samples of the low-doped manganite $La_{0.875}Sr_{0.125-x}Ca_xMnO_3$ ($0 \leqslant x \leqslant 0.125$) have been synthesized and the effect on the structural, magnetic and transport properties of decreasing the tolerance factor by replacing larger Sr^{2+} ions with smaller Ca^{2+} ions are reported. For samples with $x \geqslant 0.0625$, a concentration (x) dependent structural transition (rhombohedral ($R\bar{3}C$) to orthorhombic ($Pnma$)) has been detected at room temperature and the Curie temperature T_C is found to decrease with increased Ca doping level. For samples with $x \leqslant 0.0625$, a narrow metallic region exists and the corresponding insulator to metal transition temperature T_{MI} decreases with increasing Ca content, i.e. decreasing tolerance factor. In the paramagnetic region, x dependent crossover from Mott variable range hopping (Mott-VRH) to Shklovskii–Efros variable range hopping (SE-VRH) occurs as the Ca content increases. The thermoelectric power (TEP) of the samples increases substantially, varying inversely with the tolerance factor. These results are analysed from the consideration of increased bending of the Mn–O–Mn bond with the decrease of the average ionic radius of the A-site element $\langle r_A \rangle$ and the tolerance factor t, which causes narrowing of the bandwidth, decrease of mobility of e_g electrons and weakening of the double exchange (DE) interaction associated with the substitution of Ca.

(Some figures in this article are in colour only in the electronic version)

[3] Author to whom any correspondence should be addressed.
[4] Present address: Department of Physics, Krishnagar Women's College, Krishnagar, India.

1. Introduction

Elaborate investigations on the perovskite type rare-earth manganites having general formula $Ln_{1-x}Ae_xMnO_3$ (Ln = rare earth, Ae = alkaline earth) have highlighted two most important factors, namely hole carrier density (controlled by the Mn^{3+}/Mn^{4+} ratio) and the average ionic radius of the A-site element $\langle r_A \rangle$ [1–6], that profoundly affect the physical properties of such systems. A detailed discussion on the dependence of various properties on $\langle r_A \rangle$ invokes consideration of the geometrical quantity called the 'tolerance factor' $t = (r_A + r_O)/\sqrt{2}(r_B + r_O)$, where r_i (i = A, B or O of an ABO_3 compound) represents the average ionic size of each element. As t tends to 1, a cubic perovskite structure is expected to form. With decreasing $\langle r_A \rangle$, t also decreases and the lattice structure and other physical properties also change. An additional lattice effect is the random disorder of the trivalent and divalent cations with different sizes distributed over the $Ln_{1-x}Ae_x$ sites in the perovskite structure, which is quantified by the variance (second moment) of the A-cation radius distribution, namely σ^2 [1]. Though the size effects in moderately doped $Ln_{0.7}Ae_{0.3}MnO_3$ [6, 7] as well as in $Ln_{0.5}Ae_{0.5}MnO_3$ [3] type systems have been reported earlier, systematic study of the effect of cation size on different physical properties in low-doped manganites has not yet been well reported.

With the above picture in mind, we have synthesized a series of low-doped manganite samples, namely $La_{0.875}Sr_{0.125-x}Ca_xMnO_3$ ($0 \leqslant x \leqslant 0.125$), where the average ionic radius of the A-site, i.e. the tolerance factor t and variance, have been systematically reduced while keeping the Mn^{3+}/Mn^{4+} ratio fixed at 7. Our aim is primarily to correlate tolerance factor with various physical properties (magnetic and transport properties) of the said system. As anticipated, the structure, Curie temperature, thermoelectric and transport properties are found to be strongly influenced by the substitution of even smaller Ca^{2+} ions (ionic radius = 1.18 Å) in place of larger Sr^{2+} ions (ionic radius = 1.31 Å) elucidating the significance of A-site ionic size effects even in the low-doping regime of the manganite family.

2. Experimental details

Ceramic samples of $La_{0.875}Sr_{0.125-x}Ca_xMnO_3$ ($0 \leqslant x \leqslant 0.125$) were synthesized by the conventional solid-state reaction method in air. The precursors La_2O_3, CaO, SrO_2 and MnO_2 (each of purity better than 99.9%) were mixed in appropriate stoichiometric proportion, ground and then preheated at 1173 K for 24 h. The mixed powders thus obtained were reground, pelletized (bar shaped) and sintered at 1523 K for 12 h. The same procedure was repeated once and finally the pellets were sintered at 1773 K for another 12 h. The samples were cooled to room temperature at a rate of 2 K min^{-1}. The structures of the samples were characterized by x-ray powder diffraction (XRD) using Cu Kα radiation at room temperature. The symmetry and the lattice constants were determined by Reitveld analysis of the XRD data using the FULLPROF program [8]. A scanning electron microscope image of the sample was obtained using field emission scanning electron microscopy (JEOL JSM 6700F); energy dispersive spectroscopy (EDS) of the sample was done using the same instrument. The resistance as a function of temperature was measured by the standard four-probe method from 50 to 300 K with and without the application of an external magnetic field of 7 T. The ac susceptibility measurements were performed on a Quantum Design superconducting quantum interference device (SQUID) MPMS system from 4 to 350 K. Thermoelectric power (TEP) measurements were made by employing a differential thermocouple method using a closed cycle refrigerator within the temperature range of 80–325 K.

3. Results and discussion

3.1. Characterization

The single-phase character of all the samples was confirmed by XRD at room temperature. XRD patterns of the samples with $x = 0$ and 0.025 can be categorized by a rhombohedral

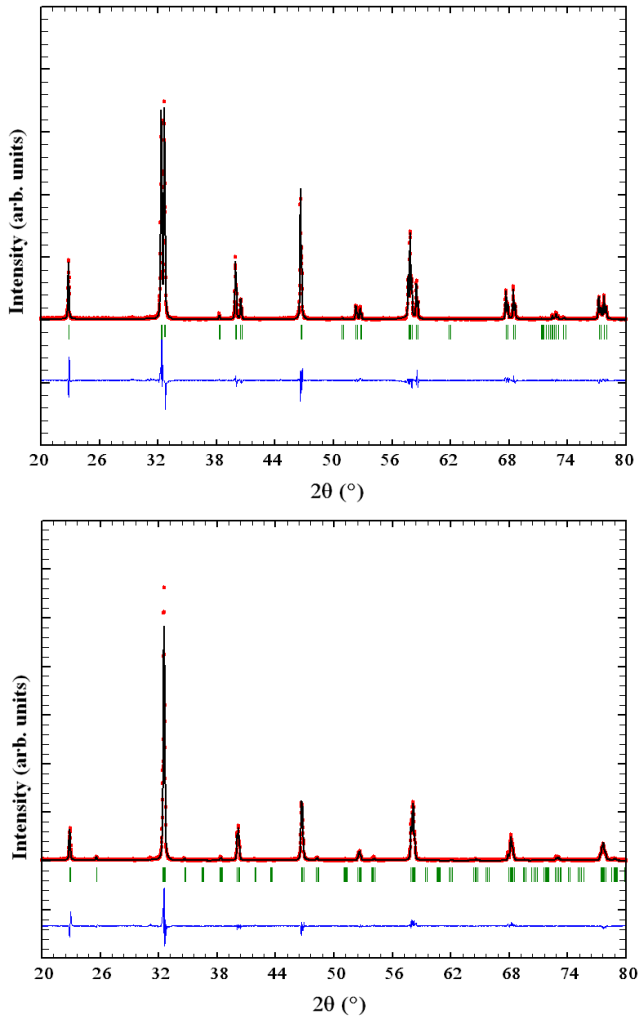

Figure 1. XRD patterns of the compound $La_{0.875}Sr_{0.125-x}Ca_xMnO_3$, with (a) $x = 0$ and (b) 0.125. The dots represent the experimental data and the calculated data are the continuous line overlapping them. The lowest curve shows the difference between the experimental and calculated patterns. The vertical bars indicate the Bragg reflection positions.

lattice with the space group $R\bar{3}C$. On the other hand, the samples with $x = 0.0625$, 0.1 and 0.125 change structure and can be indexed by an orthorhombic lattice with space group $Pnma$. Figure 1 shows experimental and calculated XRD patterns for the samples with $x = 0.0$ and 0.125. The structural parameters obtained for the sample series are listed in table 1. The orthorhombic samples exhibit a cooperative Jahn–Teller distortion of the perovskite structure. Orthorhombic perovskites can be separated into type $O^*(b/c > \sqrt{2})$, where the predominant distortion is the octahedral tilting, as in $GdFeO_3$, and type $O'(b/c < \sqrt{2})$, where the main distortion is driven by the cooperative Jahn–Teller (JT) effect, as in our samples. For $La_{0.875}Sr_{0.125-x}Ca_xMnO_3$ with $0 \leqslant x \leqslant 0.125$, the room temperature crystal structure changes from the rhombohedral phase $R\bar{3}C$ (for $x = 0.125$ and 0.1) to an orthorhombic phase $Pnma$ (for $x \leqslant 0.0625$). The lattice distortion and the bend of the Mn–O–Mn bond increase when

Table 1. Refined structural parameters (at 300 K), tolerance factor and band width of $La_{0.875}Sr_{0.125-x}Ca_xMnO_3$ ($0 \leqslant x \leqslant 0.125$). Here O(1) and O(2) denote the apical oxygen and basal plane oxygen, respectively. Brackets beside the numerals denote the standard deviation of the last digit.

Parameter	$x = 0$	$x = 0.025$	$x = 0.0625$	$x = 0.1$	$x = 0.125$
Symmetry	$R\bar{3}c$	$R\bar{3}c$	$Pnma$	$Pnma$	$Pnma$
a (Å)	5.5265(4)	5.5329(2)	5.5490(2)	5.4892(3)	5.4896(2)
b (Å)	5.5265(4)	5.5329(2)	7.7763(2)	7.7691(4)	7.7667(3)
c (Å)	13.3585(7)	13.3582(5)	5.5298(3)	5.5207(2)	5.5179(2)
v (Å^3)	353.9966(1)	353.7145(3)	238.6146(3)	235.4365(1)	235.2616(2)
Mn–O(1) (Å)	—	—	1.948(1)	1.965(5)	1.973(2)
Mn–O(2) (Å)	—	—	1.970(5)	2.011(4)	2.162(5)
Mn–O(2) (Å)	—	—	1.995(4)	1.941(4)	1.846(4)
Mn–O (Å)	1.966(2)	1.971(3)	—	—	—
Mn–O(1)–Mn (deg)	—	—	156.34(5)	162.29(1)	164.47(4)
Mn–O(2)–Mn (deg)	—	—	168.72(6)	165.02(2)	162.61(7)
Mn–O–Mn (deg)	164.06(5)	163.69(7)	—	—	—
R_p (%)	8.08	9.11	6.47	2.02	3.91
t	0.9207	0.9195	0.9178	0.9160	0.9149
W	0.092 94	0.092 08	0.091 95	0.091 91	0.088 40

the crystal structure varies from the rhombohedral to the orthorhombic lattice (table 1). It is well known that one of the possible origins of the lattice distortion of perovskite structures is the deformation of the MnO_6 octahedra originating from the JT effect that is directly related to the concentration of Mn^{3+} ions. But for the present system, where the concentration of Mn^{3+} ions is fixed, the observed lattice distortion should be caused by the average ionic radius of the A-site element $\langle r_A \rangle$ or the tolerance factor t only. As $\langle r_A \rangle$ decreases, so does t, the lattice structure transforms to a rhombohedral $R\bar{3}C$ phase and then to an orthorhombic $Pnma$ structure in which the bending of the B–O–B bond increases and the bond angle deviates from 180° [9]. For $La_{0.875}Sr_{0.125-x}Ca_xMnO_3$ (with $0 \leqslant x \leqslant 0.125$), the structural transition at room temperature mainly originates from the variation of the tolerance factor t caused by the substitution of smaller Ca^{2+} in place of larger Sr^{2+} ions. As usual, standard values of ionic radii [10] for different elements have been used to calculate $\langle r_A \rangle$ and t.

The SEM image (inset of figure 2) of a fracture surface shows the well defined character of the grains (∼8–10 μm) and grain boundary. The atomic composition of the samples was checked by EDS analysis as shown in figure 2 for the Ca-free $La_{0.875}Sr_{0.125}MnO_3$ sample only due to lack of space. The well resolved lines originating from the constituent atoms, i.e. La, Sr, Mn and O, can be observed. The chemical composition as determined by the EDS analysis shows satisfactory results within the limits of experimental error.

3.2. Magnetism

Figure 3 shows the temperature dependent real part of the ac susceptibility χ' of $La_{0.875}Sr_{0.125-x}Ca_xMnO_3$ with $0 \leqslant x \leqslant 0.125$. Upon decreasing the temperature, all the samples show a sudden increase in the value of χ' which is identified to be due to the paramagnetic to ferromagnetic transition [11, 12]. The Curie temperatures T_C (determined from the point of maximum change obtained in the $d\chi'/dT$ value) tabulated in table 2 show that T_C decreases monotonically with an increase in the Ca doping level. The reduction in T_C is attributed to the reduction of the Mn–O–Mn bond angle with decreasing average ionic radius of the A-site element $\langle r_A \rangle$, and thereby a reduction in the electron hopping between the Mn

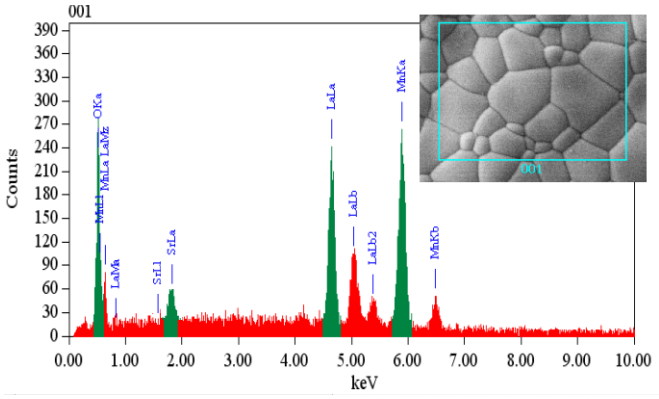

Ele...	Cl...	(keV)	mass%	Error%	At%
O K		0.525	28.39	0.22	58.09
La L		4.648	21.41	0.08	17.48
Mn K		5.894	35.10	0.18	20.92
Sr L		1.806	15.09	0.34	3.51
Total			100.00		100.00

Figure 2. Scanning electron micrograph and energy dispersive spectra of a fractured surface of $La_{0.875}Sr_{0.125}MnO_3$.

Table 2. T_C, T_{MI}, p (as described in the text) and the characteristic temperatures of SE-/Mott-VRH for the $La_{0.875}Sr_{0.125-x}Ca_xMnO_3$ ($0 \leqslant x \leqslant 0.125$) samples.

Parameter	$x = 0.125$	$x = 0.10$	$x = 0.0625$	$x = 0.025$	$x = 0$
T_C (K)	168	176	199	212	254
T_{MI} (K)	—[a]	—[a]	189	204	235
p	−0.450 97	−0.517 46	−0.386 38	−0.309 51	−0.257 88
T_0 (K)	2.12×10^4 [b]	3.10×10^4 [b]	1.41×10^5 [c]	1.33×10^6 [c]	2.43×10^8 [d]

[a] No T_{MI}.
[b] Obtained in the SE-type VRH regime.
[c] Obtained in the intermediate VRH regime.
[d] Obtained in the Mott-type VRH regime.

sites [9]. Also the DE interaction between Mn^{4+}–O–Mn^{3+} becomes weak due to the narrowing of the bandwidth (the calculated values of approximate band widths of the sample series [13] are presented in table 1) and the decrease of the mobility of e_g electrons due to the increase of Mn–O bond length and the decrease of Mn–O–Mn bond angle caused by the substitution of smaller Ca^{2+} ions for larger Sr^{2+} ions. Susceptibility is expected to diverge at ferromagnetic T_C and its value below T_C is not intrinsic to the sample; it is the demagnetization limited value for that particular sample. Actually, $1/\chi'(\text{internal}) = 1/\chi'(\text{measured}) - N$ (demagnetization factor). Hence the values of the ac susceptibility χ' cannot be compared below T_C. The χ' versus T curves for the samples with $x > 0$ show a sudden decrease at lower temperatures

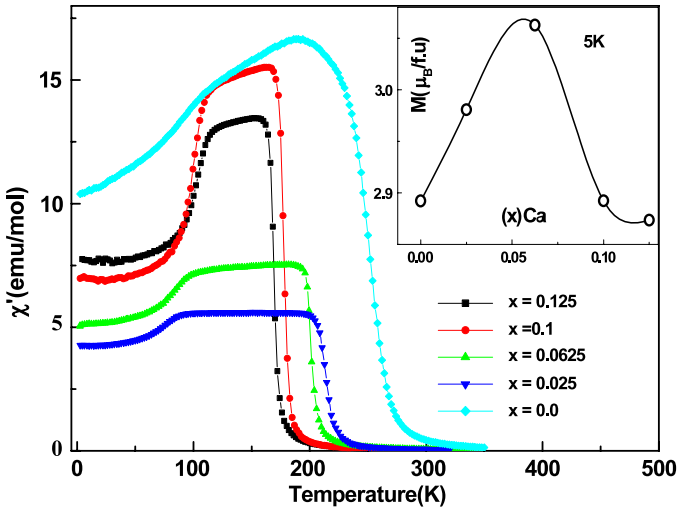

Figure 3. Thermal variation of the real part of the ac susceptibility for $La_{0.875}Sr_{0.125-x}Ca_xMnO_3$, ($0 \leqslant x \leqslant 0.125$) measured at 10 kHz.

(for instance at 97.66 K for the $x = 0.125$ sample) which looks like an antiferromagnetic transition at a first glance. But it is found from magnetization studies (discussed below) that the antiferromagnetic state is absent in the studied samples, and the decrease in the value of χ' might be due to some kind of freezing of spins or glassy nature or indicative of mere irreversible effects which can be due to the irreversible domain wall dynamics; this is beyond the scope of our discussion in this paper.

To check for a possible change of ferromagnetic fraction, isothermal ($T = 5$ K) magnetization measurements were also performed in a low magnetic field of 0.2 T. In principle, such a value is sufficient to align the ferromagnetic moments without inducing an antiferromagnetic metamagnetic transition [14]. All the values were found to be in the range of 2.8–3.0 μ_B/Mn (figure 3, inset). This indicates that all the samples of the series are almost ∼100% ferromagnetic. Clearly, the electrical localization induced by the substitution of Sr^{2+} by Ca^{2+} cannot be explained by the appearance of an insulating antiferromagnetic phase. In fact, such a substitution generates a ferromagnetic insulating (FMI) state similar to the one encountered in $Pr_{0.8}Ca_{0.2}MnO_3$ [15].

3.3. Transport properties

Figure 4 shows the temperature dependence of resistivity $\rho(T)$ for all the samples at zero field within the temperature range of 50–300 K. For the samples with $x = 0$, 0.025 and 0.0625, there exist insulator to metal transitions (T_{MI}, listed in table 2). Interestingly, peaks in the $\rho(T)$ curves are almost suppressed when a high external field (7 T) is applied, as seen from the inset of figure 4. With further Ca doping ($x > 0.0625$), the insulator to metal transition vanishes and the $\rho(T)$ curves display small inflection-like behaviour near T_C.

The above mentioned semiconducting behaviour of $\rho(T)$ curves for the samples with $x > 0.0625$, throughout the temperature range, and the increase of resistivity of the Sr-free ($x = 0.125$) sample by four orders of magnitude compared to that of the corresponding Ca-free ($x = 0.0$) sample, implies gradual enhancement of the localization of carriers [9] with increasing Ca content or in turn decreasing tolerance factor t.

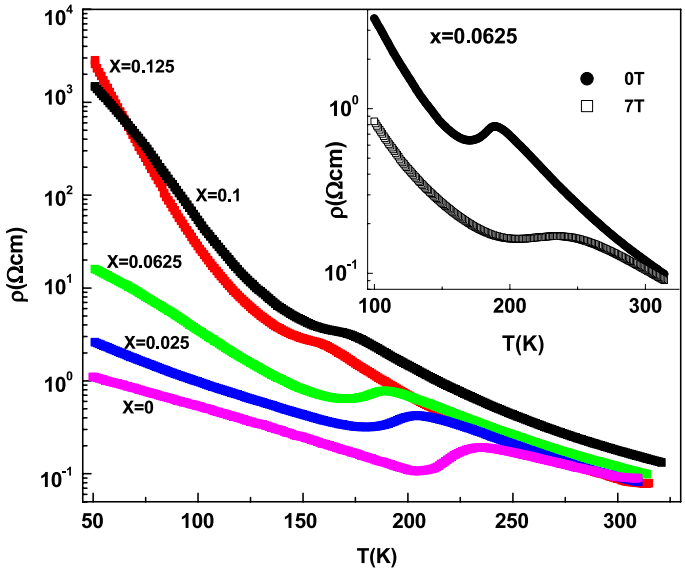

Figure 4. Thermal behaviour of the resistivity of $La_{0.875}Sr_{0.125-x}Ca_xMnO_3$ ($0 \leqslant x \leqslant 0.125$) samples measured at zero field. The inset shows the $\rho(T)$ behaviour of the $x = 0.0625$ sample at fields of 0 and 7 T.

To explain electronic conduction considering hopping conductivity over the nearest sites (NSH) an Arrhenius-like law has been proposed:

$$\rho(T) = \rho_o \exp(E_a/kT) \tag{1}$$

where the prefactor ρ_o is only a weak function of temperature and the activation energy E_a can be written in a universal form

$$E_a(T) = kT(T_0/T)^p. \tag{2}$$

In equation (2) T_0 is a constant and $p = 1, 1/4$ or $1/2$ for the NSH conductivity, the Mott-VRH [16] and the SE-VRH conductivity [17], respectively. In the SE-VRH regime, the prefactor in equation (1) $\rho_o \sim T^{1/2}$ [18], while in the Mott regime, $\rho_o \sim T^S$, where a variety of values of the exponent $s = -1/4, -3/4$ [17] or $-3/8$ [18] have been proposed depending on the details of the applied model. Therefore, to identify the type of VRH conductivity, the usual practice is to plot $\ln[T^{-1/2}\rho(T)]$ versus $T^{-1/2}$ or $\ln[\rho(T)]$ versus $T^{-1/4}$ to obtain a straight line. However, as is evident from figures 5(a) and (b), above T_C, the two plots for the LCMO sample represent straight lines of the same quality (similar plots were also made for the rest of the samples but have not been shown as they show almost the same pattern). In such a situation evaluation of the local activation energy [18]

$$E_{loc}(T) = \mathrm{d}[\ln \rho(T)]/\mathrm{d}[1/kT] \tag{3}$$

is an effective method for identifying the type of hopping. As follows from equations (1)–(3), neglecting the weak temperature dependence of ρ_o, the slope of the linear dependence of $\ln[E_{loc}(T)/kT]$ on $\ln(T)$ gives the value of $(-p)$ and hence the type of conduction law according to which the electronic conduction occurs in the paramagnetic region, as was done for the present set of samples. A constant slope with p close to $1/2$ satisfies the SE-VRH requirement. The value of $-p$ is obtained from a least square fitting. It was observed that the slope of the $\ln[E_{loc}(T)/kT]$ on $\ln[T]$ remains close to $1/2$ in the case of the sample with

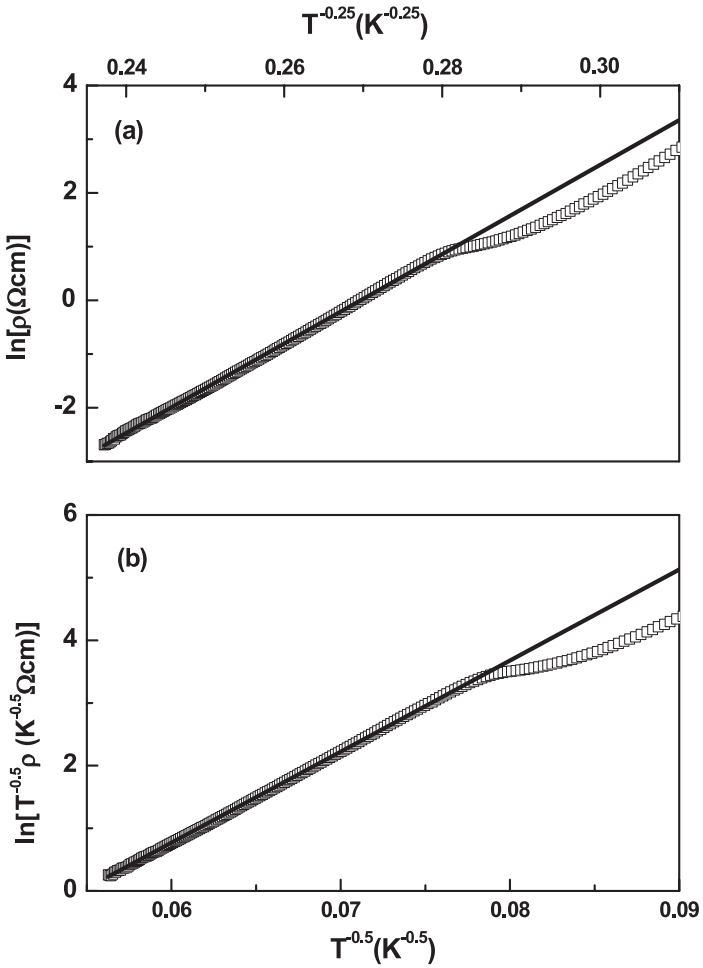

Figure 5. The resistivity versus (a) $T^{-1/2}$ and (b) $T^{-1/4}$ for the $x = 0.125$ sample. The straight line represents the fit to a linear function.

$x = 0.125$ and 0.1 only (the values obtained for all the samples are tabulated in table 2). The value of the slope decreases as the Ca content decreases and reaches a value of ~ -0.257 for the $x = 0.0$ sample, showing that a gradual transition from SE-VRH to Mott-VRH occurs with decrease in the Ca content in the case of the studied sample series. The $\ln[E_{\rm loc}(T)/kT]$ versus $\ln[T]$ curves for samples with $x = 0.125$, 0.0625 and 0.0 are shown in figure 6. The value of T_0 (characteristic SE-VRH temperature) was found from the slope of the linear dependence of $\ln[T^{-1/2}\rho(T)]$ versus $T^{-1/2}$. The characteristic VRH temperatures of the samples with $x = 0.0625$, 0.025 are determined from the slope of $\ln(\rho)$ versus $T^{(-p)}$ (value of p as determined from the $\ln[E_{\rm loc}(T)/kT]$ versus $\ln[T]$ plots) curves (shown in figure 7). The values of p and $T_{0(\rm SE-VRH\ or\ Mott-VRH)}$ are shown in table 2.

A salient question may arise here about the physical significance or reason for this gradual transition from Mott-VRH to SE-VRH conduction. The physical significance of these conduction mechanisms is that the density of states (DOS) remains constant within some interval of energy around the Fermi level in the case of Mott-VRH, while the presence of a

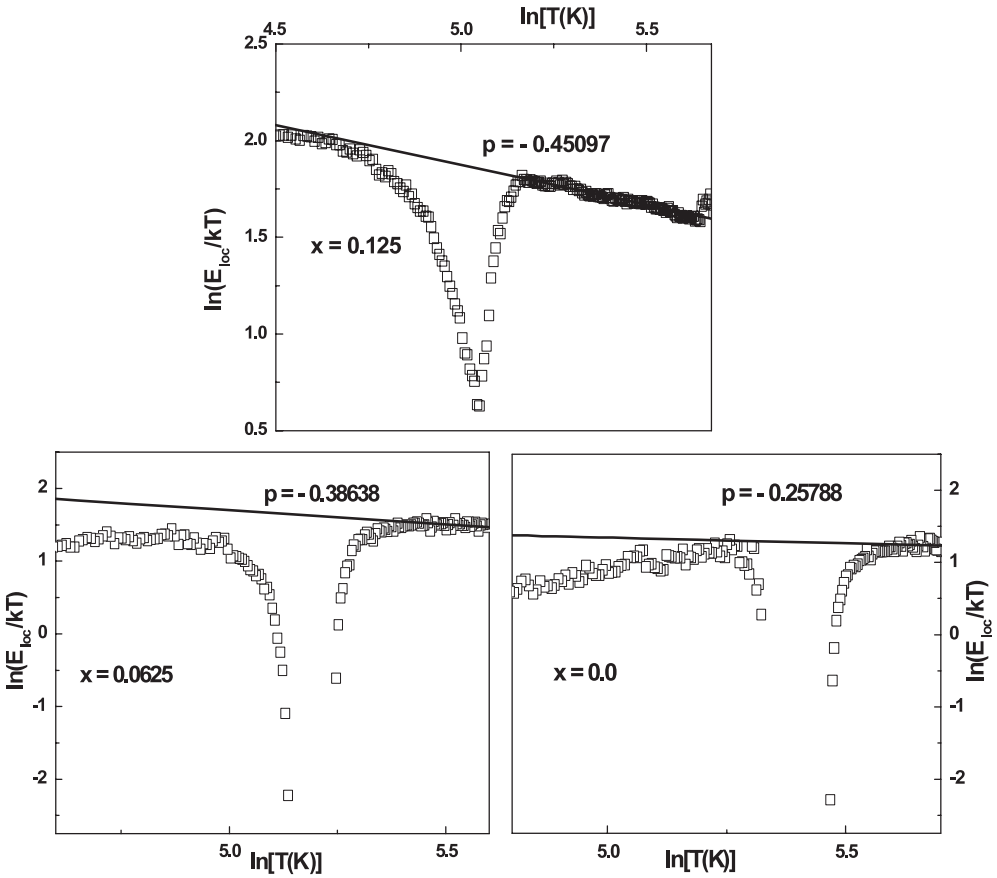

Figure 6. Local activation energy versus temperature for samples with $x = 0, 0.0625$ and 0.125. p is the angular coefficient of $\log(E_{\rm loc}/kT)$ on $\ln T$.

parabolic gap with a width (of say Δ) due to the Coulomb interaction between the localized carriers is assumed in the SE-VRH model. SE-VRH sets in when Coulomb interaction between charge carriers is important. There are various reports which show a crossover from Mott- to SE-VRH type conduction in same sample with varying temperature [19]. In a previous report Lohneysen showed in the case of compensated Si:(P, B) [20] that for VRH the long-range Coulomb interaction between an electron and a hole left behind after a hop leads to a soft Coulomb gap pinned to the Fermi energy $E_{\rm F}$, as was first recognized by Shklovskii and Efros (SE). Close to $E_{\rm F}$, the density of states varies as $D(E) \sim (E - E_{\rm F})^2$, leading to an exponent $p = 1/2$ in the T dependence of the VRH conductivity $\sigma = \sigma_{\rm o} \exp[-(T_{\rm o}/T)^{\rm p}]$ instead of $p = 1/4$ and $D(E) \sim$ constant around $E_{\rm F}$ as assumed by Mott. As screening sets in upon approaching the metal–insulator transition, the SE gap closes. Therefore, a crossover from SE- to Mott-VRH occurs as a function of N, or, at fixed N, with increasing T, where, N is the carrier concentration. Also, Zhang *et al* [21] showed crossover from Mott to SE hopping as temperature was decreased from 15 to 0.04 K for five insulating compensated n-type CdSe samples. The temperature at which crossover occurs decreases with increasing donor concentration, indicating that the Coulomb gap narrows as the metal–insulator transition is approached from the insulating side. Considering all the above reports it may be assumed that

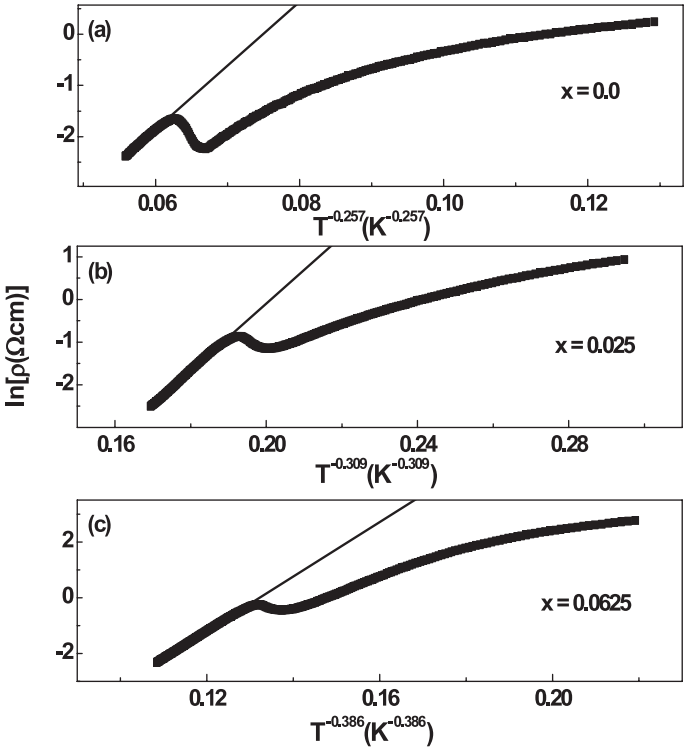

Figure 7. $\ln(\rho)$ versus T^{-p} for the $x \geqslant 0.0625$ samples. The straight line represents a linear fit.

as Ca increases in the present sample series, the samples become more insulating, i.e. carriers get more localized. Hence the Coulomb interaction among the carriers becomes significant. In the present sample series, with increasing Sr level (metal–insulator transition is observed), screening sets in and the Coulomb gap closes. So a crossover from SE- to Mott-VRH is observed.

Interesting results supporting the low temperature resistivity data are also observed from the temperature dependent thermoelectric power (TEP) measurements on the $La_{0.875}Sr_{0.125-x}Ca_xMnO_3$ samples with $x = 0$, 0.025, 0.0625, 0.1 and 0.125 as shown in figure 8. The sensitivity of TEP to the compositional variation is strongly pronounced. It is worth noting that the TEP values of all the samples are positive. Based on the TEP behaviour, two groups of samples can be separated by the borderline composition $x = 0.0625$. The samples with $0 \leqslant x \leqslant 0.0625$ have similar behaviour. It is seen that for the $x = 0.0625$ sample, the value of the Seebeck coefficient $S(\mu\text{V K}^{-1})$ starts increasing from a value of about 20.5 μV K^{-1} at 300 K to about 39.68 μV K^{-1} at 205 K (close to its PM to FM transition temperature) and falls sharply to a value of 10 at about 150 K, and finally the value of S remains almost constant until the lowest temperature is reached. For the second group of samples, as can be seen from the behaviour of the $x = 0.125$ sample in figure 7, S at 300 K is 35.03 μV K^{-1} and the value goes on increasing as temperature decreases. The value of S starts decreasing from about 69.34 μV K^{-1} at 160 K (which is again in the vicinity of the corresponding T_C), but for these samples, the decline is not as sharp as that of the first group of samples. The S value decreases gradually to 17.9 μV K^{-1} at 75 K. It is also noticed that S increases

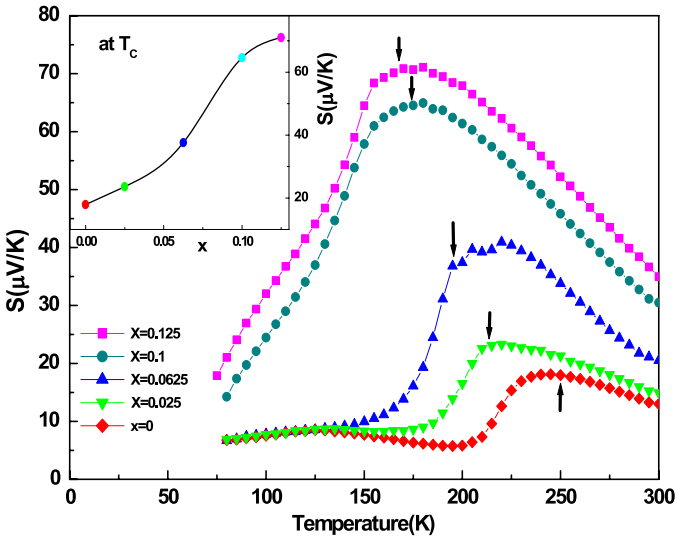

Figure 8. Temperature dependent thermoelectric power of $La_{0.875}Sr_{0.125-x}Ca_xMnO_3$ ($0 \leqslant x \leqslant 0.125$) samples. The arrows show the corresponding T_C. The $S(\mu V\ K^{-1})$ values of the samples at the corresponding T_C have been plotted against the Ca doping level in the inset.

as the Ca doping level increases, as seen clearly from the inset of figure 7 (S–x curve at corresponding T_C). Qualitatively, a decrease of TEP indicates an increase in the mobile carrier concentration [22]. Therefore, the increase in the value of S for the present samples (where Mn valency is fixed) is a signature of the localization of carriers. This result is consistent with the resistivity results discussed above. The TEP data for the samples $La_{0.875}Sr_{0.125-x}Ca_xMnO_3$, when Ca content is varied, suggest that strong electronic modification induced by the cationic size $\langle r_A \rangle$ effect is correlated to the modification in the Mn–O orbital (observed from structural data).

Summarizing the above results we can construct a phase diagram as a function of tolerance factor or variance, shown in figure 9. The T_C values of the samples decrease with the decrease in tolerance factor t. As the average A-site cationic radius $\langle r_A \rangle$ and t decrease, the lattice structure transforms from a rhombohedral $R\bar{3}C$ to an orthorhombic $Pnma$ structure. At the same time, phase transitions also occur from PMI to FMM to FMI (figure 8). All these results are associated with the increase of the bending of the Mn–O–Mn bond with the decrease of A-site cationic radius and in turn tolerance factor t because of the substitution of smaller Ca^{2+} ions in place of larger Sr^{2+}. Except for the narrow FMM phase exhibited by the samples with $x = 0$, 0.025 and 0.0625, the FMI phase dominates the phase diagram. Earlier the FMI phase had also been found in various low-doped manganite systems [23, 24]. It is to be noted that the FMI behaviour cannot be explained only on the basis of DE, as the model requires the simultaneous presence of ferromagnetism and metallicity. At low temperatures, both the FM clusters and antiferromagnetic insulating regions coexist, which contribute to the resistivity of the samples, as in the present situation the metallic clusters cannot develop into a whole network. Therefore in the present case increase of resistivity at low temperatures and thermoelectric power for the sample series where Mn valency is fixed but the cationic size varies as the Ca substitution level increases is a signature of the carrier localization corresponding to the growing fraction of ferromagnetic insulating regions.

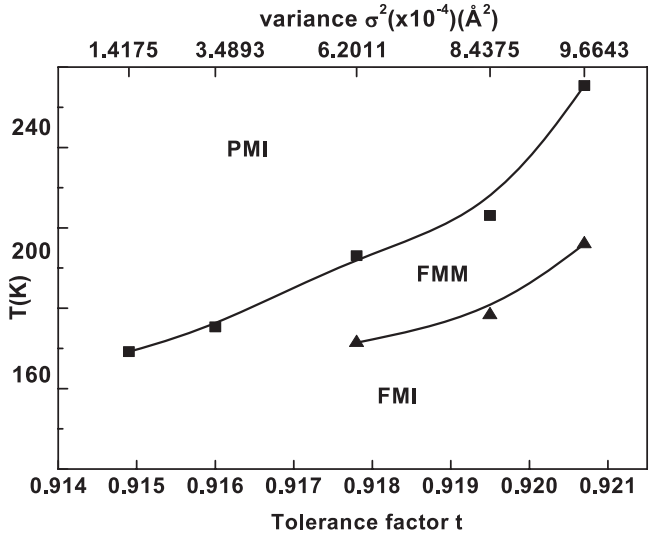

Figure 9. Phase diagram of temperature versus tolerance factor for the low-doped sample series $La_{0.875}Sr_{0.125-x}Ca_xMnO_3$, ($0 \leqslant x \leqslant 0.125$). Squares denote the Curie temperature T_C and triangles denote the metal–insulator transition temperature T_{MI}. The abbreviations used in the figure are: PMI, paramagnetic insulator; FMI, ferromagnetic insulator; FMM, ferromagnetic metal. The solid lines are guide to eyes.

4. Conclusion

The effect of Ca doping on the structural, magnetic and transport properties in the low-doped manganites series $La_{0.875}Sr_{0.125-x}Ca_xMnO_3$ ($0 \leqslant x \leqslant 0.125$) has been studied systematically. The doping of Ca in place of Sr keeps the carrier concentration fixed but varies the tolerance factor. Concentration (x) dependent room temperature structural transition from rhombohedral ($R\bar{3}C$) to orthorhombic ($Pnma$) symmetry occurs with $x \geqslant 0.0625$. All the samples undergo PM to FM transition. The Curie temperature T_C shows a linear dependence on the tolerance factor, i.e. T_C decreases with decrease in t. The insulator–metal transition disappears for samples with $x > 0.0625$ in the resistivity curves and they show insulating behaviour throughout the studied temperature range. The results of the resistivity data indicate the increase of the trend of localization of carriers as the Ca doping level increases, i.e. as t decreases. A concentration dependent gradual crossover from Mott-VRH to SE-VRH is observed in the paramagnetic region of the samples. The sample with $x = 0$ follows a Mott-VRH type conduction mechanism, while the samples with $x = 0.025$ and 0.0625 follow an intermediate VRH conduction mechanism and in samples with $x = 0.1$ and 0.125 SE-VRH type conduction prevails. The temperature dependent thermoelectric power data further support the resistivity results. The results of the present work clearly demonstrate that the structural, magnetic as well as transport properties of $La_{0.875}Sr_{0.125-x}Ca_xMnO_3$ ($0 \leqslant x \leqslant 0.125$) depend strongly on the A-site cationic radius $\langle r_A \rangle$ and the tolerance factor t of the samples. A phase diagram has also been drawn depicting the structural and magnetic transitions in the present low-doped manganite system.

Acknowledgment

The authors (BKC, EB and SK) acknowledge the Council of Scientific and Industrial Research, Government of India for financial support.

References

[1] Rodriguez-Martinez L M and Attfield J P 1996 *Phys. Rev.* B **54** R15622
[2] Barnabé A, Maignan A, Hervieu M, Damay F, Martin C and Raveau B 1997 *Appl. Phys. Lett.* **71** 3907
[3] Arulraj A, Santhosh P N, Srinivasa Gopalan R, Guha A, Raychaudhuri A K, Kumar N and Rao C N R 1998 *J. Phys.: Condens. Matter* **10** 8497
[4] Rodriguez-Martinez L M and Attfield J P 1998 *Phys. Rev.* B **58** 2426
[5] Vanitha P V, Santhosh P N, Singh R S, Rao C N R and Attfield J P 1999 *Phys. Rev.* B **59** 13539
[6] Hwang H Y, Cheong S-W, Radaelli P G, Marezio M and Batlogg B 1995 *Phys. Rev. Lett.* **75** 914
[7] Mahesh R, Mahendiran R, Chaudhuri A K and Rao C N R 1998 *J. Solid State Chem.* **120** 204
[8] Rodriquez-Carvajal J 1992 *Physica* B **192** 55
[9] Yang J, Song W H, Ma Y Q, Zhang R L, Zhao B C, Sheng Z G, Zheng G H, Dai J M and Sun Y P 2001 *Phys. Rev.* B **70** 144421
[10] Shannon R D 1976 *Acta Crystallogr.* A **32** 751
[11] Pissas M and Papavassiliou G 2004 *J. Phys.: Condens. Matter* **16** 6527
[12] Castro M, Burriel R and Cheong S W 1999 *J. Magn. Magn. Mater.* **196/197** 512
[13] Medarde M, Mesot J, Lacorre P, Rosenkranz S, Fischer P and Gobrecht K 1995 *Phys. Rev.* B **52** 9248
Radaelli P G, Iannone G, Marezio M, Hwang H Y, Cheong S-W, Jorgensen J D and Argyriou D N 1997 *Phys. Rev.* B **56** 8265
Tang F L and Zhang X 2005 *J. Phys.: Condens. Matter* **17** 6507
[14] Kim K H, Uehara M, Hess C, Sharma P A and Cheong S W 2000 *Phys. Rev. Lett.* **84** 2961
[15] Jirak Z, Krupicka S, Simsa Z, Dlouha M and Vratislav S 1985 *J. Magn. Magn. Mater.* **53** 153
[16] Mott N F and Davies E A 1979 *Electron Processes in Non-Crystalline Materials* (Oxford: Clarendon)
Mott N F 1990 *Metal–Insulator Transitions* (London: Taylor and Francis)
[17] Shklovskii B I and Efros A L 1984 *Electronic Properties of Doped Semiconductors* (Berlin: Springer)
[18] Castner T G 1991 *Hopping Transport in Solids* ed M Pollak and B Shklovskii (Amsterdam: Elsevier)
[19] Rosenbaum R 1991 *Phys. Rev.* B **56** 8265
Shen J, Chen Z, Wang N, Li W and Chen L 2006 *Appl. Phys. Lett.* **89** 153132
Arushanov E, Siebentritt S, Schedel-Niedrig T and Lux-Steiner M Ch 2006 *J. Appl. Phys.* **100** 063715
[20] Lohneysen H v 1998 *Curr. Opin. Solid State Mater. Sci.* **3** 5
[21] Zhang Y, Dai O, Levy M and Sarachik M P 1990 *Phys. Rev. Lett.* **64** 2687
[22] Taran S, Chatterjee S and Chaudhuri B K 2004 *Phys. Rev.* B **69** 184413
[23] Hejtmánek J, Jirák Z, Krupicka S, Martin C, Simon Ch, Maignan A, Raveau B, Grivei E and Issi J P 1997 *J. Appl. Phys.* **81** 4975
[24] Ye S L, Song W H, Dai J M, Wang S G, Wang K Y, Yuan C L and Sun Y P 2000 *J. Appl. Phys.* **88** 5915